Equivalence classes of Fibonacci lattices and their similarity properties

N. Lo Gullo,[1,2] L. Vittadello,[1] M. Bazzan,[1,2] and L. Dell'Anna[1,2]
[1]*Dipartimento di Fisica e Astronomia, Università degli Studi di Padova, 35131 Padova, Italy*
[2]*CNISM, Sezione di Padova, Padova 35131, Italy*
(Received 27 January 2016; revised manuscript received 8 May 2016; published 26 August 2016)

We investigate, theoretically and experimentally, the properties of Fibonacci lattices with arbitrary spacings. Different from periodic structures, the reciprocal lattice and the dynamical properties of Fibonacci lattices depend strongly on the lengths of their lattice parameters, even if the sequence of long and short segment, the Fibonacci string, is the same. In this work we show that by exploiting a self-similarity property of Fibonacci strings under a suitable composition rule, it is possible to define equivalence classes of Fibonacci lattices. We show that the diffraction patterns generated by Fibonacci lattices belonging to the same equivalence class can be rescaled to a common pattern of strong diffraction peaks thus giving to this classification a precise meaning. Furthermore we show that, through the gap labeling theorem, gaps in the energy spectra of Fibonacci crystals belonging to the same class can be labeled by the same momenta (up to a proper rescaling) and that the larger gaps correspond to the strong peaks of the diffraction spectra. This observation makes the definition of equivalence classes meaningful also for the spectral and therefore dynamical and thermodynamical properties of quasicrystals. Our results apply to the more general class of quasiperiodic lattices for which similarity under a suitable deflation rule is in order.

DOI: 10.1103/PhysRevA.94.023846

I. INTRODUCTION

Since the first experimental proof of the existence of solids lacking of translational invariance, but exhibiting a discrete Bragg diffraction spectrum [1], the study of *quasicrystals* has attracted quite a lot of attention. The impact of this discovery on the scientific community was such that in 1992 the former definition of crystal had to be modified in order to include those structures whose diffraction patterns witness long-range order yet lack translational invariance [2–4]. More generally, the study of quasiperiodic geometries has been recently the subject of different fields all devoted to the propagation of waves through quasiperiodic potentials. The spectral properties of quasicrystals have been recently used to engineer topological pumping in optical waveguides [5–7] and in ultracold gases [8,9]. Engineering of quasiperiodic structures has also been employed in optical dielectric multilayers for resonant transmission [10], solar energy harvesting [11], plasmonics [12,13], and nonlinear optics [14,15].

Dynamical and transport phenomena in this kind of structure are also radically different compared to periodic media [16–20]. For the usual periodic arrangements, dynamical and thermodynamical properties are directly related, via the Bloch theorem, to the geometry of the system. Quasiperiodic geometries, instead, lack translational invariance so that a direct relation between their structures and their dynamical properties is not generally known. It would be therefore very interesting to find a sort of classification enabling one to group together different aperiodic systems on the basis of some similarity between their geometric arrangements. In this paper we attempt to define such a classification, showing that quasiperiodic structures whose geometry is related by a suitable mathematical transformation share the main characteristics of their reciprocal lattice and of their pseudo-band structure.

II. GENERALIZED FIBONACCI LATTICES

In one dimension (1D) the paradigm of a quasicrystal is the Fibonacci lattice (FL). The FL is a 1D lattice whose adjacent points have distances belonging to the set $\{L,S\}$, standing for long and short, respectively, which are arranged according to a given sequence. Such a lattice can be constructed by means of the cut and project technique [3,4,21] thus obtaining for the coordinates of points on the real line [2] (in units of S)

$$x_n^\eta = n - 1 + \frac{1}{\eta}\left\lfloor \frac{n}{\tau} \right\rfloor, \tag{1}$$

where n is a natural positive number, $\lfloor x \rfloor$ is the integer part of x, and $\eta = S/(L-S)$. The most common instance found in literature is obtained for $\eta = \tau = (\sqrt{5}+1)/2$, the golden ratio. In this case the canonical FL (CFL) is obtained, such that the lengths are (up to a simple rescaling) $L = 1 + 1/\tau = \tau$, and $S = 1$. Nevertheless it is possible to construct Fibonacci lattices with $\eta \neq \tau$ (see Appendix A). The distances $\Delta_n = x_{n+1}^\eta - x_n^\eta$ are either $L = 1 + 1/\eta$ or $S = 1$ and they are arranged according to the Fibonacci string (FS) $LSLLSLSLLSLLSLSLLSLSL\ldots$. The latter is any word made of two letters, L and S, obtained by means of the substitution rule $S \to L$ and $L \to LS$ starting from the letter L. We notice that the position of L and S in a FS itself is independent of the parameter η and it only depends on the factor $1/\tau$.

Conversely, given an infinite FS, a composition rule ($LS \to L'$ and $L \to S'$) can be defined such that the old and the new strings are the same due to the peculiar properties of the Fibonacci strings, as shown in Fig. 1. For the special case $\eta = \tau^k$, with k a nonvanishing integer, i.e., for the CFL, this leads to a peculiar property: the new FL can be rescaled to the original one. This case is the most commonly encountered in literature, accompanied by the statement that the CFL is *self-similar*. It should be stressed, however, that this is not true for the general case $\eta \neq \tau^k$. In this case, a noncanonical Fibonacci lattice and the one obtained by applying the composition rule are characterized by two different length ratios η_1 and η_2 because $L'/L \neq S'/S$. Therefore the new lattice cannot be transformed into the old one by a simple rescaling.

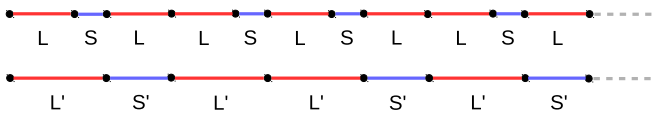

FIG. 1. The composition rules ($LS \to L'$, $L \to S'$) on a semi-infinite Fibonacci lattice reproduce another Fibonacci lattice with different lattice parameters.

We call $\mathcal{C}$ the operator corresponding to the effect of the composition rule on the FL x_n^η. It is not difficult to show that $\mathcal{C}(x_n^\eta) = \eta_1 x_n^{\eta_1}$, where $\eta_1 = 1 + 1/\eta$: the composition rule maps a FL x_n^η into another FL, characterized by a new ratio η_1 and rescaled by η_1 (see Fig. 1). If $\eta = \tau$ then $\eta_1 = \tau$ (recall that $\tau^2 - \tau - 1 = 0$) and therefore the CFL is self-similar. If the composition rule is applied k times, the initial FL is mapped into

$$\mathcal{C}^{(k)}\left(x_n^\eta\right) = \left(\prod_{i=1}^{k} \eta_i\right) x_n^{\eta_k} = \left(F_{k+1} + \frac{F_k}{\eta}\right) x_n^{\eta_k}, \qquad (2)$$

where $\eta_i = 1 + 1/\eta_{i-1}$ ($\eta_0 = \eta$) and F_k are the Fibonacci numbers. With the help of this concept we define equivalence classes for FLs by means of the following equivalence relation:

Definition. Two Fibonacci lattices $x_n^{\eta_a}$ and $x_n^{\eta_b}$ are equivalent ($x_n^{\eta_a} \sim x_n^{\eta_b}$) if they are linked, up to a proper rescaling, by means of the composition rule $\mathcal{C}$. The lattice with the minimum η_0 such that $1/(\eta_0 - 1)$ is finite and positive is called the generator of the equivalence class which is denoted by $[\eta_0]$.

A simple way of labeling the elements of a given equivalence class is by means of the continued fraction representation for the $\{\eta_i\}$.

For quasiperiodic structures it is of limited practical utility to talk about the support of the diffraction pattern. It is more meaningful to describe the diffraction spectrum (and the reciprocal lattice) in terms of the peaks which are significantly close to unity, which will be referred to as the brightest peaks. By means of the cut and project method outlined in Appendix A it is possible to show (see Appendix B) that the intensity $I(q,\eta)$ at points $q = Q(h,h')$ is given by $\mathrm{sinc}^2(Q_\perp(h,h')\Delta)$, where $Q_\perp(h,h') = 2\pi d^{-1}[h(1 + 1/\eta)^{-1} - h']$ and $\Delta = \tau[\eta/(\eta+1)]/2$. Therefore the brightest peaks are found for pairs (h,h') such that $Q_\perp(h,h') \approx 0$ and thus for (see Appendix C)

$$\frac{h}{h'} = 1 + \frac{1}{\eta}. \qquad (3)$$

Since h and h' are integers, the above condition can be satisfied exactly only if η is a rational number. On the other hand for irrational η we can resort to its continued fraction representation in order to set the wanted precision to the above condition.

Let us now consider two FLs belonging to the same equivalence class $x_n^{\eta_0}$ and $x_n^{\eta_1}$, with $\eta_1 = 1 + 1/\eta_0$. By defining h_n (k_n) and h'_n (k'_n) as the numerator and denominator of the nth rational approximants of $1 + 1/\eta_0(1 + 1/\eta_1)$, the following relations hold: $k_n = h_n + h'_n$ and $k'_n = h_n$. The position of the brightest peaks of the FL $x_n^{\eta_1}$ are then related to those of the FL $x_n^{\eta_0}$ by

$$Q_1(k_n,k'_n) = \eta_1 Q_0(h_n,h'_n). \qquad (4)$$

In other word, although the two Fibonacci lattices $x_n^{\eta_0}$ and $\mathcal{C}(x_n^{\eta_0}) = \eta_1 x_n^{\eta_1}$ cannot be rescaled one over the other (for the general case $\eta \neq \tau$), their brightest peak pattern can, as a consequence of the fact that they are related by the composition rule. Also the intensities of the brightest peaks can be related as $I(\eta_1 q,\eta_1) \approx I(q,\eta_0) + \frac{1}{\tau}[1 - I(q,\eta_0)]$ [for q such that $I(q,\eta_0) > 0.5$] showing that the peaks of the scaled lattice are even brighter than those of the original lattice. This drives one to the important conclusion that FLs belonging to the same equivalence class have diffraction spectra characterized by the same pattern of brightest peaks, and are, in this sense, similar.

III. SIMILARITY OF DIFFRACTION PATTERNS

To quantify the degree of similarity between the two spectra, we use the Kullback-Leibler divergence (KLD), a quantity useful to comparing two distributions (normalized to unity over a common support). Let us consider the diffraction spectra $I(q,\eta_\alpha)$ and $I(q,\eta_\beta)$ of two arbitrary FLs characterized by $\eta_\alpha \neq \eta_\beta$. We define the normalized spectrum as $P(\nu q,\eta) = I(\nu q,\eta)/\int_0^\infty dk I(\nu k,\eta)$ where we introduced a scaling parameter ν.

The KLD is defined as

$$D(\eta_\alpha,\eta_\beta,\nu) = \int_0^\infty dk\, P(k,\eta_\alpha) \log_{10}\left(\frac{P(k,\eta_\alpha)}{P(\nu k,\eta_\beta)}\right). \qquad (5)$$

By definition, one has that the more similar the two diffraction spectra, the smaller the value of the KLD. We will use it to measure if, for given η_α and η_β, there exists a scaling parameter ν for which the two spectra look similar.

In Figs. 2(a) and 2(b) we plot $1/D(\eta_0^\alpha,\eta,\nu)$ comparing two generators corresponding to $\eta_0^a = 6/11$ and $\eta_0^b = 1/6$ with FLs obtained from them by applying the composition rule $\mathcal{C}^{(n_\alpha)}$ respectively $n_a = 1$ and $n_b = 3$ times. The intensities $I(q,\eta)$ are evaluated by means of Eq. (B15) for lattices with $N = 300$ points. The maxima (minima of D) in the two figures correspond to $(\eta,\nu) = (\eta_1^a,\eta_1^a)$ and $(\eta,\nu) = (\eta_1^b,\eta_1^b\eta_2^b\eta_3^b)$ respectively, in agreement with Eq. (4). This shows that two FLs produce a similar diffraction pattern if and only if they can be related via Eq. (2) and therefore only if they belong to the same equivalence class.

In order to test our results on a real case, we performed a diffraction experiment on two quasiperiodic diffraction gratings prepared using a photorefractive direct laser writing (DLW) technique [22,23]. We used three gratings made up of $N = 300$ lines all written in the same substrate: (a) a periodic grating with spacing $L = 23$ μm; two Fibonacci gratings with (b) $L = 23$ μm and $S = 17$ μm ($\eta_1^a = 17/6$) and (c) $L = 23$ μm and $S = 15$ μm ($\eta_3^b = 15/8$) (For a detailed description of the experimental set up see Appendix D). So far we considered point lattices, but real structures are constituted by some physical entity (basis) arranged on the points of our quasiperiodic Fibonacci lattice. For these cases, the diffraction pattern is given by the sum in Eq. (B15) multiplied by the square modulus of a structure factor. The latter, in general, does not posses any scaling property and therefore it is necessary to correct for it when comparing different lattices. We did this experimentally by using the data of the periodic grating to extract a phenomenological expression for the structure factor as a function of q (see Appendix E). In Fig. 3(a)

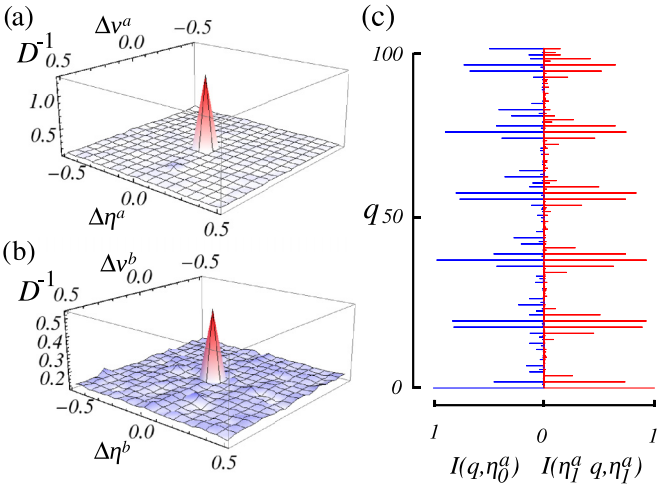

FIG. 2. Inverse of KL divergence $1/D(\eta_0^a,\eta,\nu)$ comparing the diffraction spectra of the generator of a given class $x_n^{\eta_0}$ with another Fibonacci lattice, for two choices of η_0: (a) $\eta_0^a = 6/11$ and (b) $\eta_0^b = 1/6$. Here $\Delta\eta^a = \eta - \eta_1^a$, $\Delta\nu^a = \nu - \eta_1^a$ and $\Delta\eta^b = \eta - \eta_1^b$, $\Delta\nu^b = \nu - \eta_1^b\eta_2^b\eta_3^b$. The maxima [minima of $D(\eta_\alpha,\eta_\beta,\nu)$] are obtained at $\Delta\eta^{a,b} = 0$ and $\Delta\nu^{a,b} = 0$, indicating that the two spectra with the highest degree of similarity correspond to lattices $\eta_1^a x_n^{\eta_1^a} = \mathcal{C}(x_n^{\eta_0^a})$ and $\eta_1^b\eta_2^b\eta_3^b x_n^{\eta_3^b} = \mathcal{C}^{(3)}(x_n^{\eta_0^b})$ respectively, i.e., the first and the third elements of the respective equivalence classes. (c) Direct comparison of the two diffraction spectra for two FLs $x_n^{\eta_0^a}$ and $\eta_1^a x_n^{\eta_1^a}$. The most prominent peaks of the diffraction pattern $I(q,\eta_0^a)$ correspond to those of the (rescaled) spectrum $I(\eta_1^a q,\eta_1^a)$.

we compare the experimental data relative to the grating η_1^b with the theoretical diffraction pattern obtained from the generator of the corresponding equivalence class, $\eta_0^b = 1/6$. We observe that once the spectra have been rescaled in q following Eq. (4) and corrected in order to take into account the structure factor contribution to the intensity of the peaks, the most prominent diffraction features of the generator can

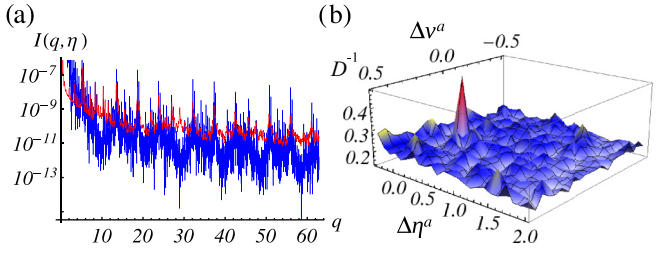

FIG. 3. (a) Comparison between the theoretical diffraction pattern for the FL $x_n^{\eta_0^a}$ ($\eta_0^a = 0.5454$, solid blue curve) and the experimental one produced by a FL $\mathcal{C}(x_n^{\eta_0^a})$ (solid red curve, $N = 300$ lines and $L = 23\ \mu$m and $S = 17\ \mu$m, $\eta_1^a = 2.8\overline{3}$). The theoretical spectrum has been rescaled in accordance with Eq. (4) and corrected for the structure factor contribution. (b) The inverse of KL divergence $[D^{-1}(\eta_1^a,\eta,\nu)]$ between the (normalized over the interval) experimental diffraction pattern and the theoretical diffraction patterns for different generators and different scaling. Here $\Delta\eta^a = \eta - \eta_0^a$ and $\Delta\nu = \nu - 1/\eta_0^a$. The maximum (minima of D) is at $(\eta,\nu) = (\eta_0^a, 1/\eta_0^a)$.

be found in the experimental data at the correct q positions. The degree of similarity between the spectrum of the generator and the experimental one is confirmed by the KL divergence D between the experimental data points and the theoretical diffraction spectrum (with the inclusion of the structure factor) calculated for a range of η_0 and scaling factor ν. In Fig. 3(b) we show it explicitly for the grating with η_1^a and it is clear that the maximum of D^{-1} (minimum of D) is found at $\eta_0 = \eta_0^\alpha$ and $\nu = \eta_1^{-1}$. Similar results are obtained for the grating η^b.

IV. ENERGY SPECTRA COMPARISON

We have therefore shown that all the FLs belonging to the same equivalence class have diffraction spectra that, although not equal, are characterized by a similar pattern of bright peaks. This finding is of crucial importance not only in scattering phenomena but also in transport ones. In fact in a recent work [24] a method to unambiguously link the gaps in the integrated density of states to the brightest peaks in the diffraction pattern of the underlying potential has been proposed. This was first observed and reported by Luck in his seminal paper [25] and is known under the name of gap labeling theorem. Let us consider for example the Hamiltonian for a particle in a 1D lattice:

$$\hat{H} = -\frac{\hbar^2}{2}\frac{d^2}{dx^2} + V(x), \tag{6}$$

$$V(x) = -V_0 \int dy f(x-y) \sum_n \delta(y - x_n), \tag{7}$$

where x_n are the local minima of the potential and $f(x)$ is introduced to account for the detailed shape of the potential minima ($V_0 > 0$). We will consider the case $x_n = x_n^\eta$ according to the quasiperiodic sequence of Eq. (1). In Ref. [24] it has been shown that it is possible to label the energy gaps by means of the brightest peaks of the diffraction spectrum. In particular one has to consider the pseudomomenta q at which the square of the Fourier transform of $V(x)$ acquires values greater than a given threshold. This effectively corresponds to choosing which free states are effectively coupled by the potential and, therefore, where wider gaps open in the single-particle spectrum. One of the results presented in Ref. [24] is that this is equivalent to setting a threshold to the intensity of the peaks in the Bragg spectrum of the lattice. This can be easily seen by considering the Fourier transform of the potential $V(x)$, namely, $V(q) = \int e^{\imath xq} V(x)dx$ whose square modulus is given by

$$|V(q)|^2 = S(q)I(q,\eta), \tag{8}$$

where $S(q)$ is the square of the Fourier transform of $f(x)$ and $I(q,\eta)$ is given by Eq. (B15). It is clear from what was shown above and confirmed by the experiment on the diffraction patterns, that apart from the contribution of the actual form of the potential (which plays a role analogous to the structure factor in diffraction experiments), the energy pseudoband structure in reciprocal space has the same shape (up to a rescaling) for the lattices belonging to a given class. As an example, we computed the spectra of Eq. (7) in the case of Gaussian wells, namely, $f(x) = e^{-x^2/2\sigma^2}$ for a system with $N = 100$ minima and $x_n = x_n^\eta$ with $\eta = \eta_0^a, \eta_1^a$ and $\eta = \eta_0^b, \eta_3^b$.

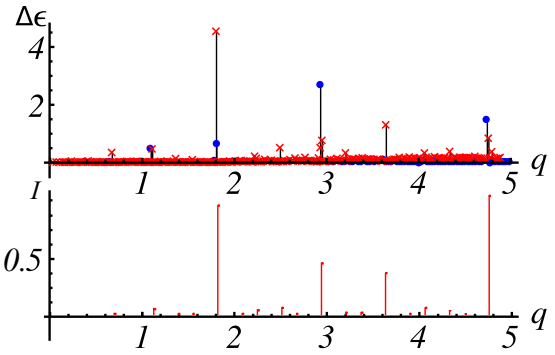

FIG. 4. Plot of the energy level spacings of the Hamiltonian in Eq. (7) for a potential $V(x)$ having minima at the points of FLs x_n^η with (blue dots) $\eta = \eta_0^a$ and (red crosses) η_1^a. Below we compare the gaps with the brightest peaks of $I(q/\eta_1^a,\eta_1^a)$.

We choose $V_0 = 12$ and $\sigma = 0.1$. In Fig. 4 we plot the energy level spacing for lattices characterized by $\eta_0^a = 6/11$ (blue dots) and $\eta_0^a = 17/6$ (red crosses) both belonging to the equivalence class $[\eta_0^a]$. The momenta on the x axis serve as a reference with respect to the free particle dispersion relation $[\epsilon_k = k^2/2, V(x) = 0]$ to show where the potential $V(x)$ opens the gaps. After rescaling the momenta for the lattices with $\eta = \eta_1^a$ by $\nu_a = \eta_1^a$ we can clearly see that the gaps appear at the same points. On the other hand these points correspond to the brightest peaks, where $I(q/\eta_1^a,\eta_1^a)$ calculated by Eq. (B15) is sizable. Similar results are obtained (not shown) for the equivalence class $[\eta_0^b]$ with $\eta_0^b = 1/6$ by considering the two lattices characterized by η_0^b and $\eta_3^b = 15/8$, under the scaling $\nu_b = \eta_1^b\eta_2^b\eta_3^b$.

V. CONCLUSIONS

In conclusion, we investigated the diffraction spectra of FLs in the general case $\eta = S/(L-S) \neq \tau$. We have shown that it is possible to group different Fibonacci lattices into equivalence classes whose elements share the main structural and dynamical properties as witnessed by their diffraction spectra and the energy gaps. These results show that the concept of equivalence classes for FLs has not only a geometrical meaning but also an important role in the scattering, dynamical, and thermodynamical properties of the system, contained in the energy spectrum. It is worth stressing once again that this is a consequence of the self-similarity of FSs under the composition rule and that FLs belonging to different equivalence classes cannot be rescaled one over the other. The generator of a class is, in this sense, the simplest structure giving a diffraction pattern which contains the main features common to all of the other elements of the class. Although we focused on the Fibonacci lattices, our arguments apply to the more general class of quasicrystals for which deflation or inflation rules can map the initial lattices into similar ones.

ACKNOWLEDGMENTS

The authors are thankful to Prof. Camilla Ferrante and Dr. Nicola Rossetto, from the Dipartimento di Chimica, Università di Padova, for providing access to the direct laser writing setup. The authors also thank J. Settino for providing the energy spectra of a particle in a Fibonacci-like lattice. N.L. and L.D. acknowledge financial support from MIUR, through FIRB Project No. RBFR12NLNA_02. L.V. and M.B. acknowledge financial support from Universit degli studi di Padova through Chip & CIOP Project No. CPDA120359.

APPENDIX A: GENERALIZED FIBONACCI LATTICES FROM CUT AND PROJECT METHOD

The Fibonacci lattices we considered in the main text can be constructed by means of the cut and project technique. One possible construction has been presented in Ref. [21]. We prefer to resort to a more standard one and in what follows we will generalize the one given in Ref. [3].

Let us introduce a two-dimensional periodic lattice $\mathcal{I}_2^p$ and its lattice vectors $\mathbf{e}_1$ and $\mathbf{e}_2$ such that any point of the lattice can be written as $\mathbf{p} = n_1\mathbf{e}_1 + n_2\mathbf{e}_2$ with $n_1,n_2 \in \mathbb{Z}$. Furthermore we introduce the line l_τ whose unit vector is $\hat{l}_\tau = [\cos(\theta_\tau), \sin(\theta_\tau)]$ and the unit vector orthogonal to it $\hat{l}_\tau^\perp = [\sin(\theta_\tau), -\cos(\theta_\tau)]$ such that $\tan(\theta_\tau) = \tau^{-1}$ where $\tau = (1+\sqrt{5})/2$. The canonical Fibonacci lattice is constructed by projecting on the line l_τ the points of a square lattice ($\mathbf{e}_1 \cdot \mathbf{e}_2 = 0$, $|\mathbf{e}_1| = |\mathbf{e}_2|$) the points whose Vonroï cell is cut by the line itself. Let us notice that with this procedure the different points are unambiguously numbered on the line l_τ once an origin and a direction have been chosen. We are going to construct our Fibonacci lattices using this definition but allowing the two-dimensional lattice to be generic as in Fig. 5. Nevertheless we will see that in order to obtain a Fibonacci lattice, namely, a one-dimensional set of points whose distances are distributed according to the Fibonacci strings and with the wanted ratio between long and short segments, we will have to restrict the set of the allowed 2D lattices. Following the discussion in Ref. [3], in order for the line $\gamma\hat{l}_\tau$ to cut the Vonroï cell centered at point $\mathbf{p}$ it has to intersect the secondary diagonal of the cell (joining the northwest to southeast point of the cell). The diagonals lie on lines parallel to $\delta(\mathbf{e}_1 - \mathbf{e}_2)$ and whose points are given by $\delta(\mathbf{e}_1 - \mathbf{e}_2) + n\mathbf{e}_1$ with $m \in \mathbb{Z}$. Their

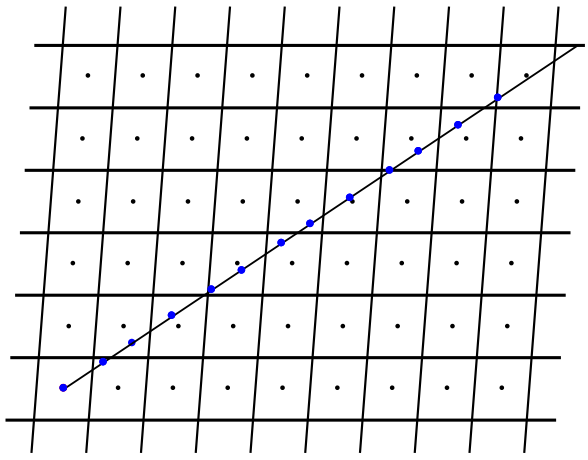

FIG. 5. Construction of a generalized Fibonacci lattice from a 2D periodic lattice by means of the cut and project method. Blue dots are the projection of points of the 2D lattice whose Vonröi cells are cut by the line l_τ.

intersection with the line $\gamma\hat{l}_\tau$ occurs at points $(\frac{n}{\tau},\frac{n}{\tau^2})a$ where $a=(\tau^2/\sqrt{1+\tau^2})A_{\text{u.c.}}/(\mathbf{e}_1-\mathbf{e}_2)\cdot\hat{l}_\tau^\perp$ and $A_{\text{u.c.}}=(\mathbf{e}_1\wedge\mathbf{e}_2)\cdot\hat{z}$ is the (oriented) area of the unit cell of the lattice.

This intersection points are inside the Vonroï cell centered at point (u,v) if and only if

$$u-\frac{|(\mathbf{e}_1-\mathbf{e}_2)\cdot\hat{x}|}{2}<n\,a\,\tau^{-1}<u+\frac{|(\mathbf{e}_1-\mathbf{e}_2)\cdot\hat{x}|}{2}, \quad \text{(A1)}$$

$$v-\frac{|(\mathbf{e}_1-\mathbf{e}_2)\cdot\hat{y}|}{2}<n\,a\,\tau^{-2}<v+\frac{|(\mathbf{e}_1-\mathbf{e}_2)\cdot\hat{y}|}{2}. \quad \text{(A2)}$$

On the other hand each point of the lattice can be written as $n_1\mathbf{e}_1+n_2\mathbf{e}_2$ and $n_1+n_2=n$ because it is the nth point to be projected. Thus we can write $u=n_1(\mathbf{e}_1-\mathbf{e}_2)\cdot\hat{x}+n\mathbf{e}_2\cdot\hat{x}$ and $v=n_1(\mathbf{e}_1-\mathbf{e}_2)\cdot\hat{y}+n\mathbf{e}_2\cdot\hat{y}$ and the above inequalities become

$$\left(n_1-\frac{s_x}{2}\right)(\mathbf{e}_1-\mathbf{e}_2)\cdot\hat{x}<n\,(a\,\tau^{-1}-\mathbf{e}_2\cdot\hat{x})<\left(n_1+\frac{s_x}{2}\right)(\mathbf{e}_1-\mathbf{e}_2)\cdot\hat{x}, \quad \text{(A3)}$$

$$\left(n_1-\frac{s_y}{2}\right)(\mathbf{e}_1-\mathbf{e}_2)\cdot\hat{y}<n\,(a\,\tau^{-2}-\mathbf{e}_2\cdot\hat{y})<\left(n_1+\frac{s_y}{2}\right)(\mathbf{e}_1-\mathbf{e}_2)\cdot\hat{y}, \quad \text{(A4)}$$

where $s_x=\text{sgn}[(\mathbf{e}_1-\mathbf{e}_2)\cdot\hat{x}]$ and similarly for s_y. By means of the expression for a it is easy to prove that $(a\,\tau^{-1}-\mathbf{e}_2\cdot\hat{x})/(\mathbf{e}_1-\mathbf{e}_2)\cdot\hat{x}=(a\,\tau^{-2}-\mathbf{e}_2\cdot\hat{y})/(\mathbf{e}_1-\mathbf{e}_2)\cdot\hat{y}$ and thus the two inequalities are equivalent to the inequality

$$\left(n_1-\frac{1}{2}\right)<\frac{n}{\beta}<\left(n_1+\frac{1}{2}\right), \quad \text{(A5)}$$

$$\beta=1-\frac{\mathbf{e}_1\cdot\hat{l}_\tau^\perp}{\mathbf{e}_2\cdot\hat{l}_\tau^\perp}=1+r\frac{1}{\tau\sin(\alpha)-\cos(\alpha)}, \quad \text{(A6)}$$

where $\cos(\alpha)=\mathbf{e}_1\cdot\mathbf{e}_2/(|\mathbf{e}_1||\mathbf{e}_2|)$ and $r=|\mathbf{e}_1|/|\mathbf{e}_2|$. With n_1 an integer number, the only possibility for the above inequalities to be satisfied is that $n_1=\lfloor\frac{n}{\beta}\rfloor$ where $\lfloor x\rfloor$ is the integer part of x. After projecting onto l_τ, the nth point has coordinates on the the line l_τ:

$$x_n'=n\,\mathbf{e}_2\cdot\hat{l}_\tau+(\mathbf{e}_1-\mathbf{e}_2)\cdot\hat{l}_\tau\left\lfloor\frac{n}{\beta}\right\rfloor. \quad \text{(A7)}$$

By normalizing with respect to $\mathbf{e}_2\cdot\hat{l}_\tau$ we eventually obtain the one-dimensional lattice of points

$$x_n=n+\frac{1}{\eta}\left\lfloor\frac{n}{\beta}\right\rfloor, \quad \text{(A8)}$$

$$\eta^{-1}=\left(\frac{\mathbf{e}_1\cdot\hat{l}_\tau}{\mathbf{e}_2\cdot\hat{l}_\tau}-1\right). \quad \text{(A9)}$$

For the above to be a Fibonacci lattice we require $\beta=\tau$ which is the case for $\tau r=[\tau\sin(\alpha)-\cos(\alpha)]$ and thus $\eta=[\tau+\tan(\alpha)]/[(\tau-1)\tan(\alpha)-\tau^2]$. Moreover we have to require that $r>0$ and $\eta>0$ which is the case for $\tan^{-1}(2\tau+1)<\alpha<\tan^{-1}(-\tau)+\pi$. As can be seen from Fig. 6, for any given $\eta>0$ there corresponds a pair (r,α):

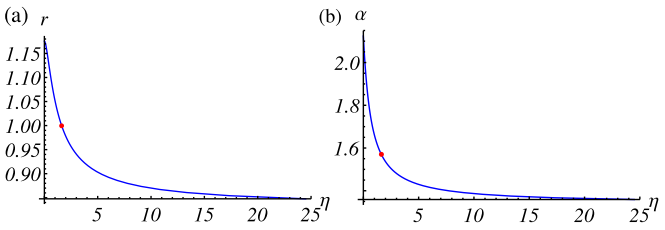

FIG. 6. (a) Values of $r=|\mathbf{e}_1|/|\mathbf{e}_2|$ as a function of η. The red dot corresponds to the point $(\eta,r)=(\tau,1)$ for which the canonical Fibonacci lattice is obtained. (b) Values of the angle α between $\mathbf{e}_1$ and $\mathbf{e}_2$ as a function of η. The red dot corresponds to the point $(\eta,\alpha)=(\tau,\pi/2)$ for which the canonical Fibonacci lattice is obtained.

$$\tan(\alpha)=\tau^2\frac{\eta\tau+1}{\eta-\tau}, \quad \text{(A10)}$$

$$r=\frac{(\tau\tan(\alpha)-1)}{\tau\sqrt{1+\tan^2(\alpha)}}, \quad \text{(A11)}$$

and therefore a two-dimensional lattice whose projection on the line l_τ returns the wanted FL:

$$x_n^\eta=n-1+\frac{1}{\eta}\left\lfloor\frac{n}{\tau}\right\rfloor, \quad \text{(A12)}$$

$$\eta^{-1}=\left(\frac{\mathbf{e}_1\cdot\hat{l}_\tau}{\mathbf{e}_2\cdot\hat{l}_\tau}-1\right), \quad \text{(A13)}$$

where we shifted the whole lattice in order for the first point to have coordinate $x_1=0$ on the line l_τ.

APPENDIX B: DIFFRACTION PATTERN

We are interested in the calculation of the quantity

$$A(q_\parallel)=\lim_{N\to\infty}\frac{1}{N}\sum_n e^{\imath x_n^\eta q_\parallel}, \quad \text{(B1)}$$

where x_n^η are given by Eq. (A13). Using the unit vectors $\hat{l}_\tau$ and $\hat{l}_\tau^\perp$ we can write any point in space as $\vec{r}=x_\parallel\hat{l}_\tau+x_\perp\hat{l}_\tau^\perp$ and similarly for the variable $\vec{q}=q_\parallel\hat{l}_\tau+q_\perp\hat{l}_\tau^\perp$. By introducing the quantity

$$A_X(q_\parallel,q_\perp)=\lim_{N\to\infty}\frac{1}{N}\sum_n e^{\imath\vec{p}_n\cdot\vec{q}}, \quad \text{(B2)}$$

where we recall that $\vec{p}_n$ are points $\vec{r}_{n_1n_2}$ of the 2D periodic lattice which lie in a strip of width $2\Delta=|(\mathbf{e}_1-\mathbf{e}_2)\cdot\hat{l}_\tau^\perp|$ around the line $\gamma\hat{l}_\tau$. It is easy to see that $A(q_\parallel)=A_X(q_\parallel,0)$. We therefore turn to the calculation of the latter. By introducing the mass density of the 2D lattice $\rho(\vec{r})=\sum_{m_1m_2}\delta(\vec{r}-\vec{r}_{m_1m_2})$ and its Fourier transform $\rho(\vec{r})=\int dk_\perp\,dk_\parallel e^{-\imath\vec{r}\cdot\vec{k}}\tilde{\rho}(\vec{k})$, we can write

$$A_X(q_\parallel,q_\perp)=\lim_{L\to\infty}\frac{1}{L}\frac{1}{2\Delta}\int dk_\perp dk_\parallel\times\int_{-\Delta}^{\Delta}dx_\perp\int_{-\infty}^{\infty}dx_\parallel\,e^{\imath\vec{r}\cdot(\vec{q}-\vec{k})}\,\tilde{\rho}(\vec{k}). \quad \text{(B3)}$$

The above integrals can be calculated as

$$A(q_\parallel) = A_X(q_\parallel,0) = \int dk_\perp \frac{\sin(k_\perp\Delta)}{k_\perp\Delta} \int dk_\parallel\, \tilde{\rho}(\vec{k})\delta(k_\parallel - q_\parallel), \quad \text{(B4)}$$

which expresses the fact that the diffraction pattern of an infinite projected quasicrystal is the convolution of the Dirac comb formed by the periodic higher dimensional periodic lattice with the sinc function in the orthogonal space.

In particular $\tilde{\rho}(\vec{k})$ is a Dirac comb peaked at points $\mathbf{k}_{hh'} = h\mathbf{w}_1 + h'\mathbf{w}_2$ where we introduced the reciprocal lattice vectors for the dual of the 2D periodic lattice $\mathcal{I}_2^p$:

$$\mathbf{w}_1 = \frac{2\pi}{l_1}(\mathbf{e}_1 - \mathbf{e}_1\cdot\hat{e}_2\hat{e}_2), \quad \text{(B5)}$$

$$\mathbf{w}_2 = \frac{2\pi}{l_2}(\mathbf{e}_2 - \mathbf{e}_2\cdot\hat{e}_1\hat{e}_1), \quad \text{(B6)}$$

$$\quad \text{(B7)}$$

where $\hat{e}_i = \mathbf{e}_i/|\mathbf{e}_i|$ and $l_1 = |\mathbf{e}_1|^2 - |\mathbf{e}_1\cdot\hat{e}_2|^2$ and similarly for l_2. It is easy to check that $\mathbf{w}_i\cdot\mathbf{e}_j = 2\pi\delta_{ij}$. In what follows we assume that units are scaled such that $\mathbf{e}_2\cdot\hat{l}_\tau = 1$. In order to evaluate the parallel and perpendicular components of vectors belonging to the reciprocal space we need to evaluate $\mathbf{w}_i\cdot\hat{l}_\tau$ and $\mathbf{w}_i\cdot\hat{l}_\tau^\perp$. To do so it is useful to rewrite the vectors $\mathbf{e}_i$ as linear combinations of $\hat{l}_\tau$ and $\hat{l}_\tau^\perp$ by means of the expressions for η and β and the relation between $\tan\alpha$ and η. We thus obtain

$$\mathbf{e}_1 = \left(1+\frac{1}{\eta}\right)\hat{l}_\tau + \frac{1}{\tau}\left(1+\frac{1}{\eta}\right)\hat{l}_\tau^\perp, \quad \text{(B8)}$$

$$\mathbf{e}_2 = \hat{l}_\tau - \left(1+\frac{1}{\eta}\right)\hat{l}_\tau^\perp. \quad \text{(B9)}$$

It is now easy to check that

$$\mathbf{w}_1\cdot\hat{l}_\tau = \frac{2\pi}{d}, \quad \mathbf{w}_2\cdot\hat{l}_\tau = \frac{2\pi}{\tau d}, \quad \text{(B10)}$$

$$\mathbf{w}_1\cdot\hat{l}_\tau^\perp = \frac{2\pi}{d\left(1+\frac{1}{\eta}\right)}, \quad \mathbf{w}_2\cdot\hat{l}_\tau^\perp = -\frac{2\pi}{d}, \quad \text{(B11)}$$

where $d = (\tau + 1/\eta)$. Therefore we can define

$$Q(h,h') = \mathbf{k}_{hh'}\cdot\hat{l}_\tau = \frac{2\pi}{d}\left(h + \frac{h'}{\tau}\right), \quad \text{(B12)}$$

$$Q_\perp(h,h') = \mathbf{k}_{hh'}\cdot\hat{l}_\tau^\perp = \frac{2\pi}{d}\left(\frac{\eta\, h}{\eta+1} - h'\right). \quad \text{(B13)}$$

By means of Eq. (B4) we can thus write the intensities of the diffracted points as

$$I(q_\parallel,\eta) = |A(q_\parallel)|^2 = \sum_{h,h'} \frac{\sin^2[Q_\perp(h,h')\Delta]}{[Q_\perp(h,h')\Delta]^2}\delta(q_\parallel - Q(h,h')), \quad \text{(B14)}$$

where $\Delta = \tau(1+1/\eta)/2$ and we introduce the explicit dependence of the intensity on the parameter η which characterizes the FL. As it can be seen, the diffraction spectrum consists of a set of sharp peaks centered on a dense set of reciprocal lattice points, as by choosing the appropriate values of h and h', any q can be approximated with arbitrary precision. However, not all these peaks have the same intensity.

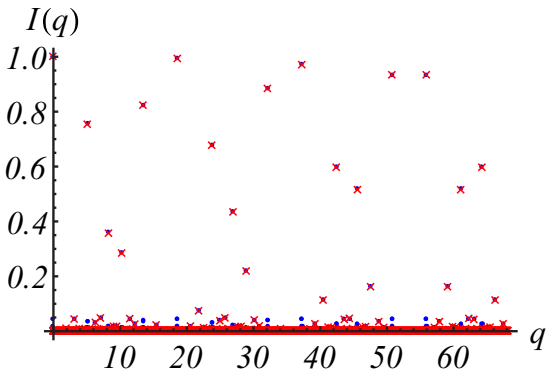

FIG. 7. Comparison between the values of $I(q_\parallel)$ using the cut and project method and the direct evaluation in Eq. (B1) for a lattice of $N = 300$ points and $\eta = 17/6$. Blue dots are points corresponding to the value in Eq. (B14) whereas red crosses are given by Eq. (B1).

In Fig. 7 we plot $I(q_\parallel)$ as given by expression in Eq. (B14) and its expression calculated explicitly by its definition Eq. (B1) for a lattice of $N = 300$ points and $\eta = 17/6$. We can see that as expected the peak intensities are well captured by Eq. (B14) even for finite systems especially for peaks characterized by a significant intensity (>0.2).

We now consider the (Fraunhofer) diffraction pattern of a FL x_n^η:

$$I(q,\eta) = \lim_{N\to\infty}\frac{1}{N^2}\left|\sum_n e^{\imath x_n^\eta q}\right|^2. \quad \text{(B15)}$$

This quantity is important because it gives a direct experimental access to the reciprocal lattice of our structure. We shall see that this quantity is also encountered in the determination of a (pseudo) energy dispersion relation [24]. In the case of FLs the values of q at which a nonvanishing intensity is expected are given by

$$Q(h,h') = \frac{2\pi}{d}\left(h + \frac{h'}{\tau}\right), \quad \text{(B16)}$$

where $d = (\tau + 1/\eta)$. By properly choosing the integers h and h', any real number can be arbitrarily well approximated, showing that the reciprocal lattice of a FL is dense in $\mathbb{R}$, contrary to periodic lattices which exhibit a discrete reciprocal lattice. Moreover it can be shown [3] that the diffraction pattern has *only* pure point support, lacking a continuous part (according to the classification of positive measures in the Lebesgue classification).

APPENDIX C: BRIGHTEST PEAKS

1. Condition for brightest peaks

To find the set of points in reciprocal space corresponding to a strong diffracted intensity for a FL, the following condition on the argument of the exponential in the expression for the diffraction pattern has to hold:

$$Q_\perp(h,h') \approx 0, \quad \text{(C1)}$$

which is satisfied for

$$\frac{h}{h'} \approx 1 + \frac{1}{\eta}. \tag{C2}$$

Let us now consider the equivalence class $[\eta_0]$ and in particular the sequence $x_n^{\eta_0}$. We can write η_0 in the continued fraction representation

$$\eta_0 = a_0 + \cfrac{1}{a_1 + \cfrac{1}{a_2 + \cfrac{1}{a_3 + \cdots}}} \equiv [a_0, a_1, a_2, a_3, \ldots]. \tag{C3}$$

For a rational number the sequence of numbers a_i is finite, namely, $\eta_0 = [a_0, a_1, \ldots, a_n]$. On the other hand, if η_0 is irrational, it is possible to find a rational approximation within the wanted error by increasing the number of terms in its continued fraction representation. It is easy to see that $\eta_1 = 1 + 1/\eta_0 = [1, a_0, a_1, \ldots]$ and in general

$$\eta_k = [\underbrace{1, 1, \ldots, 1}_{k}, a_0, a_1, \ldots]. \tag{C4}$$

With this notation is straightforward to see that regardless of the value of the generator η_0, the sequences of an equivalence class will tend to a Fibonacci sequence since $\lim_{k\to\infty} \eta_k = [1,1,1,1,\ldots] = \tau$ [26]. Using the continued fraction notation we can write a sequence of rational approximants to η_0 as a_0, $\frac{a_1 a_0 + 1}{a_1}$, $\frac{a_2(a_1 a_0 + 1) + a_0}{a_2 a_1 + 1}$, ... Since both h and h' have to be integers, the above condition (C2) is satisfied if we choose $h = s_n + t_n$ and $h' = s_n$ where s_n and t_n are the nth approximants of η_0, namely, $\eta_0 \approx s_n/t_n$ and can easily be derived from the continued fraction representation of η_0.

It is worth stressing that if η_0 is a rational number ($\eta_0 = a/b$, with $a, b \in \mathbb{N}$) h and h' can be chosen such that $h/h' = (a + b)/a$. Thus, at points $q_m = Q(m(a+b), mb) = 2m\pi$ ($m \in \mathbb{Z}$) we have that $I(q_m, \eta_0) = 1$. On the other hand, for irrational η_0 the condition is never satisfied exactly but we can resort to the rational approximants of η_0 to estimate the positions at which the brightest peaks appear.

2. Relation between positions of brightest peaks

Let $x_n^{\eta_0}$ and $x_n^{\eta_1}$ be two Fibonacci lattices belonging to the same equivalence class and their associated reciprocal lattices $Q_0(h,h') = 2\pi d_0^{-1}(h + h'/\tau)$ and $Q_1(h,h') = 2\pi d_1^{-1}(k + k'/\tau)$, respectively, where $d_i = \tau + 1/\eta_i$. By defining h_n (k_n) and h'_n (k'_n) as the numerator and denominator of the nth rational approximants of $1 + 1/\eta_0$ ($1 + 1/\eta_1$), the following relations hold true: $k_n = h_n + h'_n$ and $k'_n = h_n$. By inserting these relations into the expression for $Q_1(k,k')$ we get

$$\begin{aligned} Q_1(k_n, k'_n) &= \frac{2\pi}{d_1}\left(k_n + \frac{k'_n}{\tau}\right) = \frac{2\pi}{d_1}\left(h_n + h'_n + \frac{h_n}{\tau}\right) \\ &= \frac{2\pi\tau}{d_1}\left(h_n + \frac{h'_n}{\tau}\right) = \frac{d_0\tau}{d_1}\frac{2\pi}{d_0}\left(h_n + \frac{h'_n}{\tau}\right) \\ &= \frac{d_0\tau}{d_1} Q_0(h_n, h'_n) = \eta_1 Q_0(h_n, h'_n), \end{aligned}$$

where in the last line we used the fact that $d_0\tau/d_1 = \eta_1$. This means that the lattice obtained by applying the composition rule $\mathcal{C}(x_n^{\eta_0}) = \eta_1 x_n^{\eta_1}$ has the brightest peaks at the same positions of the original lattice only rescaled by a factor η_1.

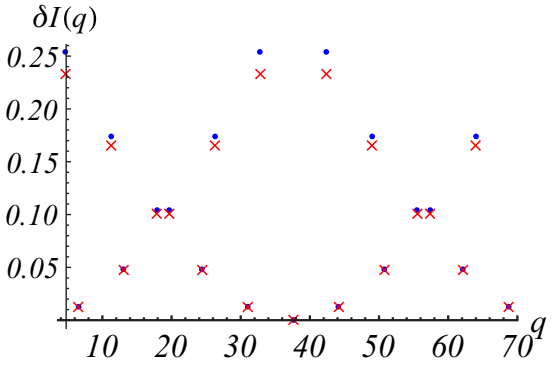

FIG. 8. Plot of (blue dots) $\tau^{-1}[1 - I(q,\eta_0)]$ and (red crosses) $[I(\eta_1 q, \eta_1) - I(q,\eta_0)]$ for those q for which $I(q,\eta_0) > 0.5$ showing that the intensities of the brightest peaks of the diffraction pattern of a FL $x_n^{\eta_1}$ generated from a FL $x_n^{\eta_0}$ by means of the composition rule are more intense than those of the original lattice by a factor of τ.

3. Relation between intensities of brightest peaks

From Eq. (B14) we can also estimate the relation between the intensities of the brightest peaks in the diffraction spectrum of two FLs belonging to the same class. Using the expression in Eq. (B14) and assuming $k_\perp \Delta \approx 0$ we can write $\sin^2(k_\perp\Delta)/(k_\perp\Delta)^2 - 1 \approx (k_\perp\Delta)^2/9$. Using the condition for $k_\perp \approx 0$ and following a calculation similar to that to determine the relation between the positions of the brightest peaks we find that $(k_\perp^1 \Delta_1)^2 = (k_\perp^0 \Delta_0)^2/\tau^2$. Therefore we have

$$I(\eta_1 q, \eta_1) \approx I(q,\eta_0) + \frac{1}{\tau}[1 - I(q,\eta_0)], \tag{C5}$$

meaning that the intensities of the brightest peaks of the scaled lattice are more intense than those of the original lattice by a term proportional to the difference between the maximum attainable intensity and the intensity of the original lattice intensities.

In Fig. 8 we plot the quantities (blue dots) $\tau^{-1}[1 - I(q,\eta_0)]$ and (red crosses) $[I(\eta_1 q, \eta_1) - I(q,\eta_0)]$ for q such that $I(q,\eta_0) > 0.5$ and for lattices of $N = 300$ sites and $\eta_0 = 6/11$ and $\eta_1 = 1 + 1/\eta_0$ respectively.

APPENDIX D: EXPERIMENTAL SETUP

To test experimentally the diffraction from FLs, a series of quasiperiodic diffraction gratings were prepared using a photorefractive direct laser writing (DLW) technique [22]. This technique consists of scanning with a focused laser beam a photorefractive sample, and engraving on it a series of lines with a modified refractive index with respect to the rest of the sample. The scanning movement is performed by translating the sample with the aid of a computer-controlled XY stage at constant speed of 50 μm/s. The nominal precision of the translation stage is 0.5 μm for the conditions used in this experiment. A frequency doubled diode pumped Nd:YWO_4 solid-state laser (Coherent Verdi V5) emitting a cw beam at 532 nm was used as the light source for DLW. The beam was suitably attenuated by a series of neutral density filters and sent to a focusing microscope objective (Olympus 100X/0.80) so that the power after the objective

was set at 17 mW. The substrate used to engrave the optical structures is a slab of photorefractive lithium niobate doped with iron at the nominal concentration of 0.1 mol% in the melt. The sample was X-cut with dimensions (X × Y × Z) $1 \times 8 \times 13$ mm^3 and the lines were written on the X face, by scanning along the Y direction with an ordinarily polarized beam.

This process can induce extraordinary refractive index changes as large as 10^{-3} in the written lines and therefore can be used to produce arbitrary diffraction structures. The diffraction pattern of these structures was measured with the help of a computer-controlled optical diffractometer in which the sample and the detector were mounted on two coaxial goniometers that were independently controlled by a computer [23]. An optical beam produced by a He-Ne laser at 632.8 nm with a power of 4 mW was expanded, polarized along the extraordinary direction, and finally transmitted through the sample surface, resulting in a clearly visible diffraction pattern. This pattern was measured by a Si photodiode and a lockin amplifier and recorded on the computer as a function of the detector and the sample angle.

APPENDIX E: EXPERIMENTAL DIFFRACTION PATTERNS

1. Structure factor

To compare the experimental data with the theoretical calculation we need to take into account that our gratings are made up of a (quasi) periodic repetition of a region with a modified refractive index, $\Delta n(x)$. This leads to the fact, well known from standard diffraction theory, that the diffracted intensity in reciprocal space is proportional to the product of two terms: a first one, $S(q) = |\int \Delta n(x) e^{\imath x q} dx|^2$ which depends on the detailed structure of the repeated unit of the grating (*structure factor*) and a second term related to lattice geometry, which is the true object of this study:

$$I_R(q,\eta) = S(q)\frac{1}{N^2}\left|\sum_n e^{\imath x_n^\eta q}\right|^2 = S(q)I(q,\eta). \qquad \text{(E1)}$$

The structure factor modulates the intensity of the lattice diffraction pattern, complicating the comparison between experiments and theory. In principle $S(q)$ could be calculated by knowing the details of the refractive index profile changes produced by our technique. Here we used another approach which exploits the fact that our samples differ only for the line position sequence x_n. We can use therefore the periodic grating (Fig. 9) to measure the function $S(q)$ directly at the reciprocal lattice points $\{q_M^i\}$ of the periodic grating, where $I(q_M^i)$ has local maxima.

We found that the following phenomenological functional form for $S(q)$ describes adequately the peak intensity in the whole range of measured values (see Fig. 9):

$$S(q) = S_0 e^{-\lambda q - \frac{q_0}{q}}, \qquad \text{(E2)}$$

where the parameters S_0, λ, q_0 are determined by a least-squares fit in the range $q \in [0.5,3]$ μm^{-1} excluding the last peaks, because the corresponding momenta were comparable with a length scale of the order of the optical waveguide width. We also notice that all measured diffraction patterns drop almost to zero outside the interval $q \in [-4,4]$ μm^{-1}; this is because our lines have a width determined by the laser writing optics which is not smaller than 2 μm, so our diffraction pattern cannot probe $|q| > 3$ μm^{-1}.

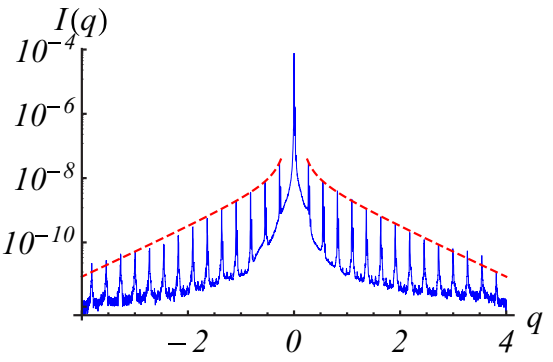

FIG. 9. Experimental diffraction pattern of the periodic grating with spacing $L = 23$ μm (blue, solid curve) and fit of the satellite peak intensities using function (E2) (red, dashed curve).

2. Comparison with theoretical patterns

In Fig. 10 we compare the theoretical diffraction pattern $I(q,\eta)$ with the experimental data points for the grating η_3^b. The intensity of the experimental points has been rescaled to take into account the contribution of the structure factor of the grating, and the q axis of the experimental plot has been rescaled in order to compare it with the simulation, which considers FLs with $S = 1$. A similar figure is obtained for the case $\eta_1^a = 17/6$. The agreement is very satisfactory: not only the position but also the intensity of the diffraction peaks are correctly obtained, confirming that our approach is reliable.

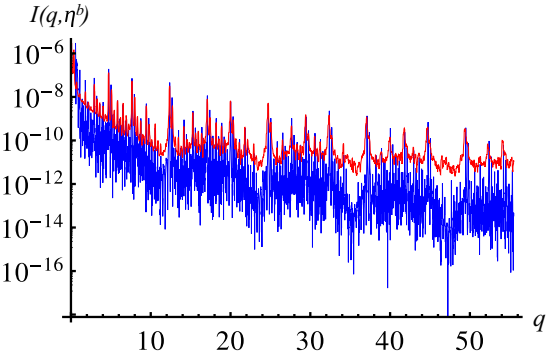

FIG. 10. Experimental diffraction pattern (solid red top curve) compared with the theoretical diffraction pattern with the inclusion of the structure factor (solid blue bottom curve) for a Fibonacci grating with $N = 300$ lines and $L = 23$ μm and $S = 15$ μm, $\eta_3^b = 1.875$.

[1] D. Shechtman, I. Blech, D. Gratias, and J. W. Cahn, Phys. Rev. Lett. **53**, 1951 (1984).

[2] D. Levine and P. J. Steinhardt, Phys. Rev. B **34**, 596 (1986).

[3] M. Senechal, *Quasicrystals and Geometry* (Cambridge University, New York, 1995).

[4] C. Janot, *Quasicrystals. A Primer*, 2nd ed. (Oxford University, Oxford, 1994).

[5] Y. E. Kraus and O. Zilberberg, Phys. Rev. Lett. **109**, 116404 (2012).

[6] Y. E. Kraus, Y. Lahini, Z. Ringel, M. Verbin, and O. Zilberberg, Phys. Rev. Lett. **109**, 106402 (2012).

[7] M. Verbin, O. Zilberberg, Y. E. Kraus, Y. Lahini, and Y. Silberberg, Phys. Rev. Lett. **110**, 076403 (2013).

[8] M. Lohse, C. Schweizer, O. Zilberberg, M. Aidelsburger, and I. Bloch, Nat. Phys. **12**, 350 (2016).

[9] K. Singh, K. Saha, S. A. Parameswaran, and D. M. Weld, Phys. Rev. A **92**, 063426 (2015).

[10] R. W. Peng, Y. M. Liu, X. Q. Huang, F. Qiu, M. Wang, A. Hu, S. S. Jiang, D. Feng, L. Z. Ouyang, and J. Zou, Phys. Rev. B **69**, 165109 (2004).

[11] A. Lin, Y. K. Zhong, S. M. Fu, C. W. Tseng, and S. L. Yan, Opt. Express **22**, A880 (2014).

[12] A. Gopinath, S. V. Boriskina, N.-N. Feng, B. M. Reinhard, and L. Dal Negro, Nano Lett. **8**, 2423 (2008).

[13] X. Huang, and M. L. Brongersma, Nano Lett. **13**, 5420 (2013).

[14] Y. W. Lee, F. C. Fan, Y. C. Huang, B. Y. Gu, B. Z. Dong, and M. H. Chou, Opt. Lett. **27**, 2191 (2002).

[15] P. Y. Chou, W. K. Chang, H. P. Chung, and Y. H. Chen, Opt. Express **22**, 28857 (2014).

[16] N. D. Lanzillotti-Kimura, A. Fainstein, B. Jusserand, A. Lemaitre, O. Mauguin, and L. Largeau, Phys. Rev. B **76**, 174301 (2007).

[17] A. R. Overy, A. B. Cairns, M. J. Cliffe, M. G. Tucker, and A. L. Goodwin, Nat. Commun. **7**, 10445 (2016).

[18] Ch. Li, H. Cheng, R. Chen, Tian. Ma, Li-G. Wang, Yu. Song, and Hai-Q. Lin, Appl. Phys. Lett. **103**, 172106 (2013).

[19] *Optics of Aperiodic Structures: Fundamentals and Device Applications*, edited by L. Dal Negro (Pan Stanford, Singapore, 2014).

[20] *Collective Dynamics of Nonlinear and Disordered Systems*, edited by G. Radons, W. Just and P. Hussler (Springer-Verlag, Berlin, 2005).

[21] P. Buczek, L. Sadun, and J. Wolny, Acta Phys. Pol. B **36**, 919 (2005).

[22] L. Vittadello, A. Zaltron, N. Argiolas, M. Bazzan, N. Rossetto, and R. Signorini, J. Phys. D **49**, 125103 (2016).

[23] M. Bazzan, N. Argiolas, C. Sada, P. Mazzoldi, S. Grilli, P. Ferraro, P. De Natale, and L. Sansone, Ferroelectrics **352**, 25 (2007).

[24] J.-M. Gambaudo and P. Vignolo, New J. Phys. **16**, 043013 (2014).

[25] J.-M. Luck, Phys. Rev. B **39**, 5834 (1989).

[26] This can also be seen by explicit calculation, in fact it is possible to show that $\eta_k = \frac{F_{k+1}\eta_0+F_k}{F_k\eta_0+F_{k-1}}$, where F_k are the Fibonacci numbers ($F_0 = 0$). The above expression tends to τ as $k \to \infty$ due to the fact that $F_{k+1}/F_k \to \tau$ in this limit.